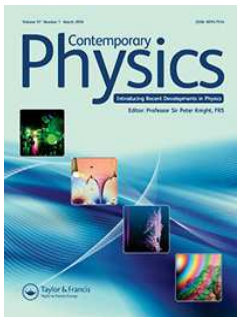

Contemporary Physics

ISSN: 0010-7514 (Print) 1366-5812 (Online) Journal homepage: http://www.tandfonline.com/loi/tcph20

Photo-induced superconductivity

Andrea Cavalleri

To cite this article: Andrea Cavalleri (2017): Photo-induced superconductivity, Contemporary Physics, DOI: 10.1080/00107514.2017.1406623

To link to this article: https://doi.org/10.1080/00107514.2017.1406623

Published online: 11 Dec 2017.

CONTEMPORARY PHYSICS, 2017
https://doi.org/10.1080/00107514.2017.1406623

Taylor & Francis
Taylor & Francis Group

Photo-induced superconductivity

Andrea Cavalleri[a,b]

[a]Max Planck Institute for the Structure and Dynamics of Matter, Hamburg, Germany; [b]Clarendon Laboratory, Department of Physics, Oxford University, Oxford, UK

ABSTRACT

Recent advances in laser technology have made it possible to generate of precisely shaped strong-field pulses at terahertz frequencies. These pulses are especially useful to selectively drive collective modes of solids, for example, to drive materials in a fashion similar to what done in the synthetic environment of optical lattices. One of the most interesting applications involves the creation of non-equilibrium phases with new emergent properties. Here, I discuss coherent control of the lattice to favour superconductivity at 'ultra-high' temperatures, sometimes far above the thermodynamic critical temperature T_c.

ARTICLE HISTORY
Received 21 September 2017
Accepted 13 November 2017

KEYWORDS
Superconductivity; ultrafast science; nonlinear phononics; structural dynamics

1. Introduction

Ultrashort laser pulses at near-infrared and visible photon energies (0.5–3 eV, i.e. 10^2–10^3 THz frequency) are routinely used to perturb materials, measuring their relaxation rates and pathways as well as inducing new properties not found at equilibrium.

In the case of complex solids with strongly correlated electrons, optical excitation has been especially effective because it can redistribute charges amongst different orbitals, tipping the balance between competing forms of order. Photo-induced insulator-to-metal transitions [1–6], control of magnetic [7] and orbital [8] orders have been widely discussed in the literature.

However, in most cases eV-energy photons cannot effectively control cooperative physics that occurs at meV scales, because high-temperature electron distributions are induced (1 eV – 14,000 K), which in turn generate large amounts of heat through incoherent scattering [9,10].

In Figure 1, we report a schematic classification of elementary excitations in complex solids, along with the corresponding energy scales. Infrared-active phonons and local vibrational modes of molecular solids can be typically reached with optical pulses (5–20 μm wavelength, 50–250 meV photon energy, 15–50 THz frequency). At lower frequencies in the single-THz range (~300 μm wavelength, ~few meV photon energy), collective modes from broken symmetry states are found. Recent developments in generation of intense laser pulses of sub-picosecond duration at mid-infrared (MIR) and terahertz (THz) frequencies [11] have opened up the non-linear excitation of these low-energy modes [12].

2. Coherent control of the crystal lattice

The linear response of a crystal lattice to a resonant light field is determined by the potential energy $H_{lin} = \frac{1}{2}\omega_{IR}^2 Q_{IR}^2$. In this expression, Q_{IR} is the normal mode coordinate and ω_{IR} its eigenfrequency. When resonantly driven by a pulsed field $f(t) = F(t)\sin(\omega_{IR}t)$ (being $F(t)$ a Gaussian envelope), the dynamics can be described by the equation of motion of a damped harmonic oscillator

$$\ddot{Q}_{IR} + 2\gamma_{IR}\dot{Q}_{IR} + \omega_{IR}^2 Q_{IR} = f(t),$$

where γ_{IR} is the damping constant. After stimulation, the atoms start to oscillate about their equilibrium positions along the normal mode coordinate and then relax over a timescale set by either the envelope duration or by the decay time $1/\gamma_{IR}$.

We then turn to 'strong' electric fields, larger than ~1 MV/cm, that is when oscillatory atomic motions extend beyond 1% of the equilibrium lattice constant. In this case, anharmonic coupling to other modes with generic coordinate Q_R becomes important. To the lowest order, the lattice Hamiltonian describing the non-linear interaction reads

$$H = \frac{1}{2}\omega_R^2 Q_R^2 - a_{12} Q_{IR} Q_R^2 - a_{21} Q_{IR}^2 Q_R,$$

CONTACT Andrea Cavalleri andrea.cavalleri@mpsd.mpg.de

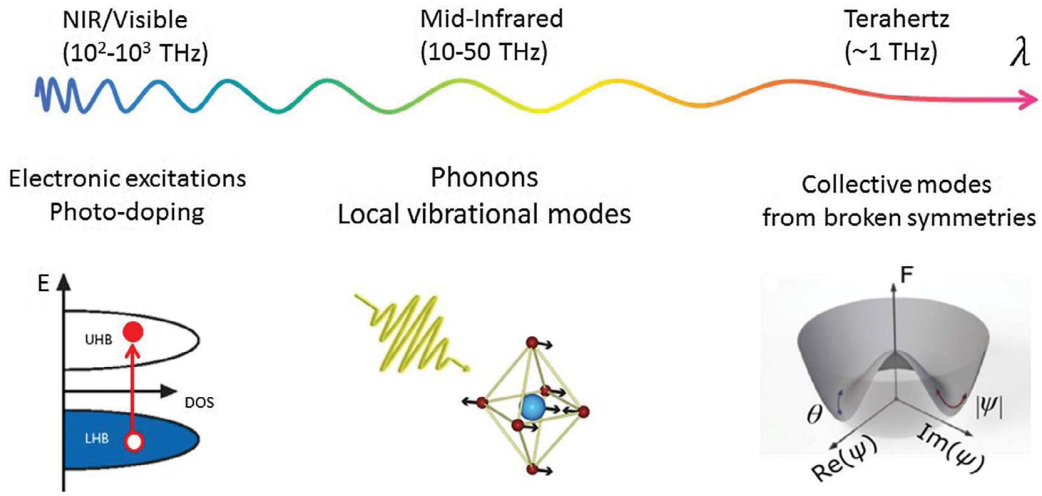

Figure 1. Energy scales of the fundamental excitations of solids in the visible and infrared. Whereas, light pulses at near-infrared and visible frequencies (102–103 THz) drive electronic transitions, phonons and other collective modes can be excited at MIR and THz frequencies.

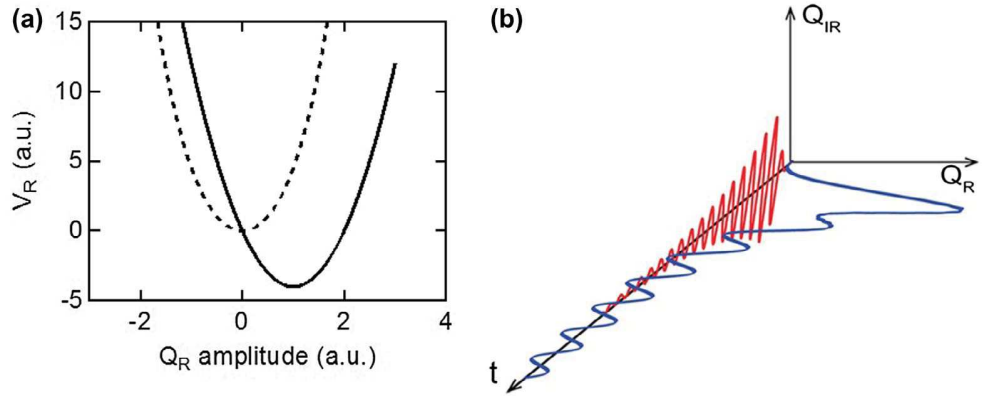

Figure 2. (a) Energy potential V_R for a Raman-active phonon mode (dashed curve). Within cubic coupling, this energy potential shifts towards a new position (solid curve) for finite static displacement of a coupled IR-active mode Q_{IR}. (b) Dynamical response of the two coupled modes. The ions oscillate coherently along the IR-active mode coordinate Q_{IR} (red) and undergo a directional displacement along Q_R, with a displacement scaling as Q_{IR}^2. If optical excitation is fast compared to the Raman phonon period, also coherent oscillations along Q_R take place.

where a_{ij} are the anharmonic coupling constants.

In the case of centrosymmetric crystals, for which IR-active phonons have odd parity, while Raman-active modes are even, the first coupling term $a_{12}Q_{IR}Q_R^2$ is always zero (for symmetry reasons) and the second term $a_{21}Q_{IR}^2Q_R$ is nonzero only if Q_R is a Raman mode. For a finite displacement Q_{IR}, a shift of the Raman mode's energy potential V_R along its coordinate Q_R is induced, as depicted in Figure 2(a). This phenomenon was analysed theoretically in the 1970s and named 'Ionic Raman scattering' [13–15].

The dynamics following excitation of the IR-active mode are described by the two coupled equations of motion

$$\ddot{Q}_{IR} + 2\gamma_{IR}\dot{Q}_{IR} + \omega_{IR}^2 Q_{IR} = 2a_{21}Q_{IR}Q_R + f(t),$$

$$\ddot{Q}_R + 2\gamma_R\dot{Q}_R + \omega_R^2 Q_R = a_{21}Q_{IR}^2.$$

The Raman mode Q_R is then subject to a force $a_{21}Q_{IR}^2$, with its direction being independent of the sign of Q_{IR}. Hence, the atoms of the crystal lattice are not only made to oscillate along the IR coordinate Q_{IR}, but are simultaneously also displaced along the Raman coordinate Q_R, as schematically depicted in Figure 2(b).

These lowest order non-linear phonon effects were demonstrated in a number of materials, including manganites [16,17] and ferroelectrics [18]. These physics was also extensively applied to experiments in which specific bonds were targeted to drive electronic phase transitions through selective changes in lattice arrangements

[19–21]. Amongst these applications, an important strand of research has been one in which specific electronic symmetries can be broken with light. In the following, we review work in which non-linear phononics has been used to enhance electronic coherence in unconventional high-temperature superconductors.

3. Photo-induced superconductivity in the cuprates

3.1. High-temperature superconductivity in the cuprates

High-T_c superconductivity emerges in single-layer cuprate of the type of the type La_2CuO_4 when a few per cent excess charges are injected, for example, by doping with Sr or Ba. A schematic drawing of a cuprate crystal structure is reported in Figure 3. The key unit of these structures is the *ab* plane, in which Cu atoms surrounded by four oxygens dominate the physics. The extraordinary feature of these materials is that, despite their ceramic character, poor conductivity in the normal state and the proximity to insulating phases, they become superconducting when cooled below high critical temperatures [22]. Depending on the compound T_c can range between 30 and nearly 200 K.

Immediately after the discovery of high-T_c cuprates, P.W. Anderson pointed out [23] a few unique features of these materials. Firstly, these materials are strongly correlated Mott insulators, and are close to an antiferromagnetic state. A Mott insulator is a material in which the conductivity vanishes, even though band theory would predict it to be metallic.

Many examples of Mott insulators are known, including NiO, $LaTiO_3$ and V_2O_3. A Mott insulator is fundamentally different from a conventional (band) insulator. In the latter, conductivity is blocked by the Pauli exclusion principle. When the highest occupied band contains two electrons per unit cell, electrons cannot move because all orbitals are filled. In a Mott insulator, charge conduction is blocked instead by electron–electron repulsion. When the highest occupied band contains only one electron per unit cell, electron motion requires creation of a doubly occupied site. If the electron–electron repulsion is strong enough, this motion is blocked. The amount of charge per cell becomes fixed, leaving only the electron spin on each site to fluctuate. Doping restores electrical conductivity by creating sites to which electrons can jump without incurring a cost in Coulomb repulsion energy. The high-T_c cuprates are highly unconventional versions of Mott insulators, which rather than metallic become superconducting when the electron concentration is changed from one per cell.

Secondly, Anderson reasoned, the electronic properties of these materials are two dimensional, because the doped charges reside in the planes and the coupling between those is small. Hence, their fluctuations are especially large. He proposed that the quantum fluctuations of a two-dimensional spin ½ system like the parent compound La_2CuO_4 or for low doping values might be sufficient to destroy long-range spin order.

The resulting 'spin liquid' would contain electron pairs whose spins are locked in an antiparallel or 'singlet' configuration. It was also pointed out that the valence bonds resemble the Cooper pairs of Bardeen–Cooper–Schrieffer

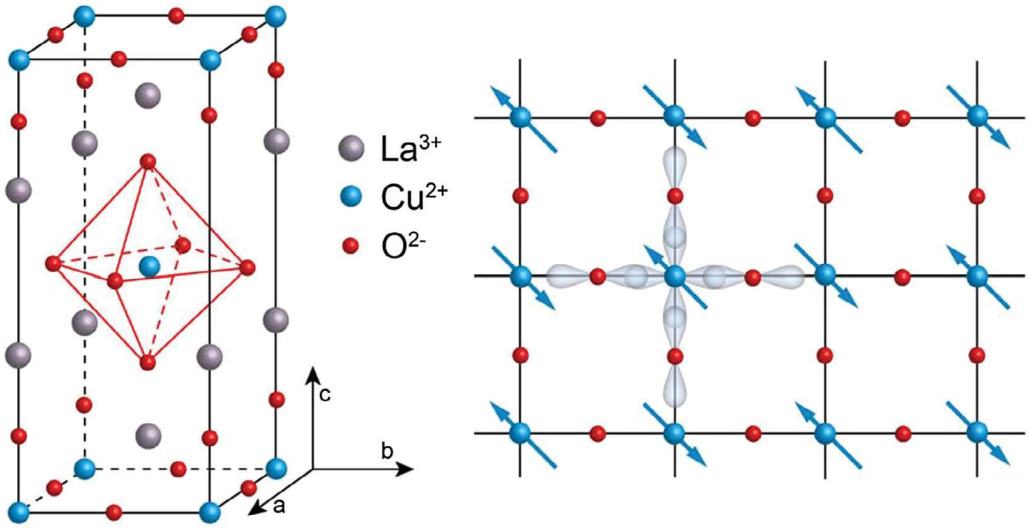

Figure 3. (a) Crystal structure of La_2CuO_4, the 'parent compound' of the $La_{(2-x)}Sr_xCuO_4$ family of high-temperature superconductors. Doping is achieved by substituting Sr ions. (b) Schematic of CuO_2 plane, the crucial structural subunit for high-T_c superconductivity. In grey, we find oxygen 'pσ orbitals'; responsible for the superexchange interaction.

(BCS) superconductivity. Because the Mott insulator is naturally paired, Anderson argued, it would become superconducting if the average occupancy is lowered from one. One aspect of the Anderson early proposal that has survived the test of time is that the magnetic properties are keys to the physics of cuprates. Indeed, virtual charge fluctuations in a Mott insulator generate negative exchange interaction, which favours antiparallel alignment of neighbouring spins. In many materials, this leads to long-range antiferromagnetic order. The spins order in a commensurate antiferromagnetic pattern at a high Néel temperature between 250 and 400 K. The extent of the antiferromagnetic phase in the temperature versus carrier concentration plane of the high-T_c phase diagram is illustrated in Figure 4 (see green section of the phase diagram). The Néel temperature drops very rapidly as the average occupancy is reduced from 1 to $1 - x$, reaching zero at a critical doping x c of only 0.02 in the $La_{(2-x)}Ba_xCuO_4$ system, for example. As the doping increases, the magnetic order reduces and the superconducting state emerges.

In the last few years, it became clear that inhomogeneous spin and charge ordering, more colloquially known as *stripe*s was found in these systems. Indeed, as shown in Figure 4, superconductivity is found for hole concentrations $x > 0.05$, reaching the maximum T_c at $x \simeq 0.16$. The region of the phase diagram around $x = 1/8$ is also characterised by the periodic one-dimensional modulation of charge and spin density (the so-called *stripes*) [24,25], which causes a reduction in T_c [26,27]. In $La_{2-x}Ba_xCuO_4$, these stripes become static at 1/8-doping, thanks to a periodic buckling of the CuO_2 planes in a low-temperature tetragonal (LTT) phase [28–30]. Static stripes, LTT phases and suppressed superconductivity are also detected in other single-layer cuprates, such as $La_{1.8-x}Eu_{0.2}Sr_xCuO_4$ [31,32]. A typical crystal structure for these compounds is displayed in Figure 3(a), a compound for which the superconducting critical temperature is strongly reduced for all doping values $x < 1/8$ and completely suppressed at $x = 1/8$ (see Figure 3(b)) [33,34].

While stripes are typically pinned by the LTT distorted structure and compete with superconductivity, recent experiments performed under external pressure have revealed the presence of stripes without any LTT distortion [35,36], underscoring the notion that charge ordering alone may be driving the microscopic physics [37]. Even more strikingly, recent experiments [38,39] have suggested that the individual striped planes may in fact be in a highly coherent paired state, a so-called *pair density wave*, in which the stripes (see Figure 3(c)) modulate the superconducting order parameter in plane and frustrate the interlayer coherent transport. This notion is supported by new experimental work based on non-linear optical spectroscopy at terahertz frequencies [40].

It is also helpful to briefly discuss here how superconductivity is destroyed either by raising temperature or by changing doping. There is wide agreement on the determining factor for T_c in underdoped materials, largely due to the pioneering experiments of Uemura and collaborators [41] and some insightful theory and phenomenology. Uemura et al. found that, unlike in the conventional superconductors studied before the discovery of the cuprates, T_c is not proportional to the gap but to the zero-temperature

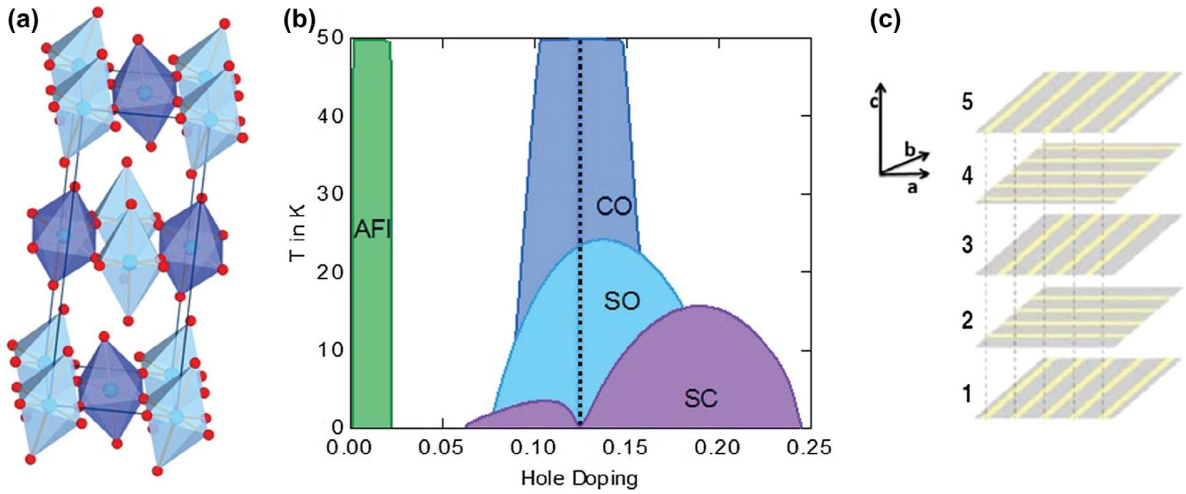

Figure 4. (a) Schematic crystal structure and (b) phase diagram for $La_{1.8-x}Eu_{0.2}Sr_xCuO_4$. The concentration of Sr (x) corresponds to hole doping. This compound is an antiferromagnetic insulator at $x = 0$. A low-temperature tetragonal (LTT) distortion, associated with buckling of the CuO_2 planes, quenches superconductivity at $x = 1/8$ (vertical dashed line), and reduces it a lower hole doping levels. At this doping, a one-dimensional modulation of charges (CO) and spins (SO), the stripe state, emerges in the planes. At $x > 1/8$, the compound is superconducting. (c) Periodic stacking of CuO_2 planes in the stripe phase. The stripe orientation rotates by 90° between layers, thus preventing interlayer superconducting phase coherence.

superfluid density (or phase stiffness) ρ_s ($T = 0$) for a wide range of underdoped materials.

This observation was discossed by many groups, although it was formulated in a very general context by Emery and Kivelson [42], who clarified how a conventional superconductor has two important energy scales: the BCS gap Δ, which measures the strength of the binding of electrons into Cooper pairs, and the phase stiffness ρ_s, which measures the ability of the superconducting state to carry a supercurrent. In conventional superconductors, Δ is much smaller than ρ_s and the destruction of superconductivity begins with the breakup of electron pairs. However, in cuprates the two energy scales are more closely balanced; when the temperature exceeds $\sim\rho_s$, thermal agitation will destroy the ability of the superconductor to carry a supercurrent, while the pairs continue to exist; thus, T_c is bounded above by a pure number times $\rho_s(T = 0)$. With time it has become clear that superconductivity is reduced by phase fluctuations, although quasiparticles play a crucial role in weakening the phase stiffness.

3.2. Restoring superconductivity in the striped phase

Recently, non-linear phononics has been exploited to control this competition dynamically in the 1/8-doped, non-superconducting $La_{1.675}Eu_{0.2}Sr_{0.125}CuO_4$. The crystal lattice was driven through an IR-active Cu–O stretch in the plane of the stripes [43]. The resulting non-equilibrium state was shown to be superconducting by time-resolved THz spectroscopy. Note that at equilibrium, superconductivity in layered cuprates is reflected in the appearance of a Josephson plasma resonance (JPR) in the *c*-axis THz optical properties [44], a feature that is well understood by considering that tunnelling between stacks of two-dimensional superconducting CuO_2 layers [45–47]. Figure 5(a) displays the equilibrium *c*-axis reflectivity of $La_{1.84}Sr_{0.16}CuO_4$ ($T_c = 35$ K), measured below and above the critical temperature. The JPR appears as an edge near 60 cm^{-1} (~2 THz). In the normal state, for which interlayer transport is resistive, the response is featureless. The equilibrium THz reflectivity of non-superconducting $La_{1.675}Eu_{0.2}Sr_{0.125}CuO_4$ at 10 K, shown in Figure 5(b), is also featureless.

Figure 5(c) reports the THz reflectivity of $La_{1.675}Eu_{0.2}Sr_{0.125}CuO_4$ measured at $\tau = +5$ ps after excitation of the Cu–O stretching mode. A reflectivity edge was measured at the same 2-THz frequency reported for $La_{1.84}Sr_{0.16}CuO_4$ at equilibrium, indicative of non-equilibrium superconducting transport.

Note that the measured transient edge is only 0.1% in amplitude, due to the pump–probe penetration depth mismatch. At THz frequencies, the probe pulse interrogates a volume that is between 10^2 and 10^3 times larger than the transformed region beneath the surface, with this mismatch being a function of frequency. This mismatch was taken into account by modelling the response of the system as that of a photo-excited thin layer on top of an unperturbed bulk (which retains the optical properties of the sample at equilibrium).

The connection between the light enhancement of superconductivity and the melting stripes, which quench the superconducting state at equilibrium, was tested with a soft X-ray Free Electron Laser (Stanford LCLS) by femtosecond resonant soft X-ray diffraction in the compound $La_{1.875}Ba_{0.125}CuO_4$ [48]. Both static stripe order and the LTT distortion were measured through resonant diffraction near the oxygen K-edge. Here, static charge stripes can be observed at the $\boldsymbol{q}$ = (0.24 0 0.5) wave vector [30,49,50], whilst the LTT distortion can be directly measured at the (0 0 1) diffraction peak [51].

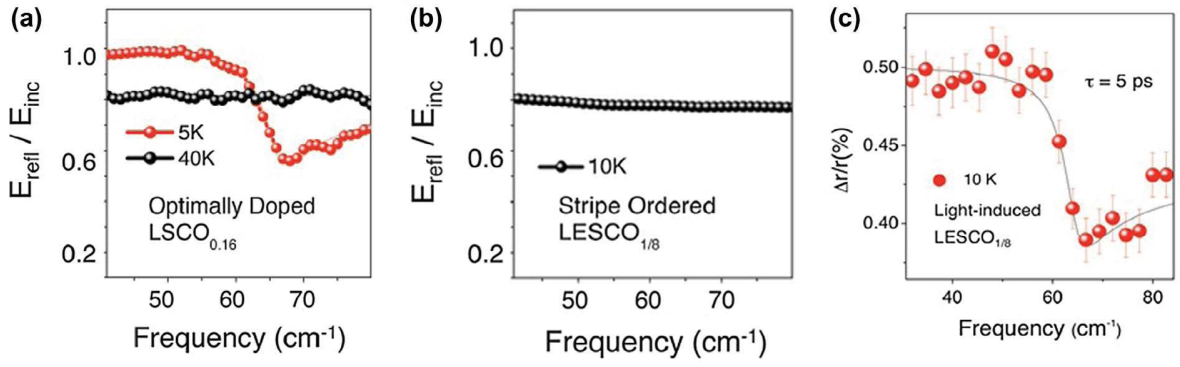

Figure 5. (a) Equilibrium *c*-axis reflectivity of $La_{1.84}Sr_{0.16}CuO_4$ ($T_c = 35$ K). In the superconducting state, the appearance of a JPR reflects coherent interlayer transport. Above T_c, incoherent ohmic transport is reflected by a flat and featureless spectrum. (b) Equilibrium *c*-axis reflectivity of $La_{1.675}Eu_{0.2}Sr_{0.125}CuO_4$ at 10 K, showing the response of a non-superconducting compound. (c) Reflectivity changes induced in $La_{1.675}Eu_{0.2}Sr_{0.125}CuO_4$ by MIR excitation at 10 K, showing a light-induced JPR.

MIR pulses, tuned to the IR-active in-plane Cu–O stretching phonon [52], were used for excitation of the sample, which was kept at a base temperature of 15 K. The time-dependent integrated scattering intensity of the (0.24 0 0.5) stripe order diffraction peak in response to the MIR excitation is plotted in Figure 6(a), and displays a prompt decrease of ~70%. This result shows that stripe order is melted within less than 1 ps, a timescale similar to that observed for the onset of superconductivity in the $La_{1.675}Eu_{0.2}Sr_{0.125}CuO_4$ [43]. This strongly suggests that stripe melting and light-induced superconductivity are intimately connected.

In contrast, the evolution of the LTT phase, probed by the (0 0 1) diffraction peak drops by only 12%, and with a much longer time constant of ~15 ps, likely determined by acoustic propagation and expansion of the lattice planes (see Figure 6(b)). Hence, the same direct lattice excitation that induces superconducting interlayer tunnelling between striped planes also melts charge-stripe order, whereas it initially leaves the LTT distortion intact.

3.3. Light-induced superconductivity far above T_c in the bilayer cuprates

New aspects of the physics emerge when analysing other types of cuprate superconductors. Enhancement of superconductivity was not only observed in the striped phases of single-layer compounds, but over a far broader doping and temperature range in the bilayer high-T_c cuprate $YBa_2Cu_3O_x$.

Orthorhombic $YBa_2Cu_3O_x$ is made up of bilayers of CuO_2 planes, separated by insulating Yttrium layers (Figure 7(a)). The bilayers are further spaced by Cu–O chains, which control the hole doping in the CuO_2 planes. In analogy with what reported for single-layer compounds, the coherent inter-bilayer tunnelling of Cooper pairs in the superconducting state of $YBa_2Cu_3O_x$ results in the appearance of a JPR in the *c*-axis THz optical response. This appears as an edge in the reflectivity, as shown in Figure 7(b) for the three hole concentrations investigated ($x = 6.45$, 7% holes, $T_c = 35$ K; $x = 6.5$, 9% holes, $T_c = 50$ K; $x = 6.6$, 12% holes, $T_c = 62$ K), all belonging to the 'underdoped' region of the phase diagram, i.e. the region with doping concentrations lower than that giving the maximum T_c (~16%).

The $YBa_2Cu_3O_x$ single crystals were photo-excited with MIR pulses tuned to be resonant with a phonon mode of B_{1u} symmetry, which involves oscillations of the so-called 'apical' oxygen atoms (see Figure 7(a)). Note that the static atomic position of these apical oxygen atoms, and in particular their distance from the CuO_2 planes, is known to be an important parameter in high-T_c cuprates, which affects the in-plane band structure and correlates strongly with the maximum achievable T_c within each cuprate family [53]. It is therefore to be expected that large-amplitude oscillations of these atoms driven by the MIR pulses have dramatic effects on the superconducting response of $YBa_2Cu_3O_x$.

The transient response measured after excitation below T_c (i.e. in the superconducting state) is summarised in Figure 8(a)–(c). At all measured dopings and all $T < T_c$, a pump-induced increase in the imaginary conductivity was measured, suggestive of an enhancement of inter-bilayer superconducting coupling. Note that this response is by far different and opposite in phase from that measured after non-resonant electronic excitation at near-infrared and optical frequencies [54,55], where only a depletion of superfluid density due to Cooper pair breaking was observed.

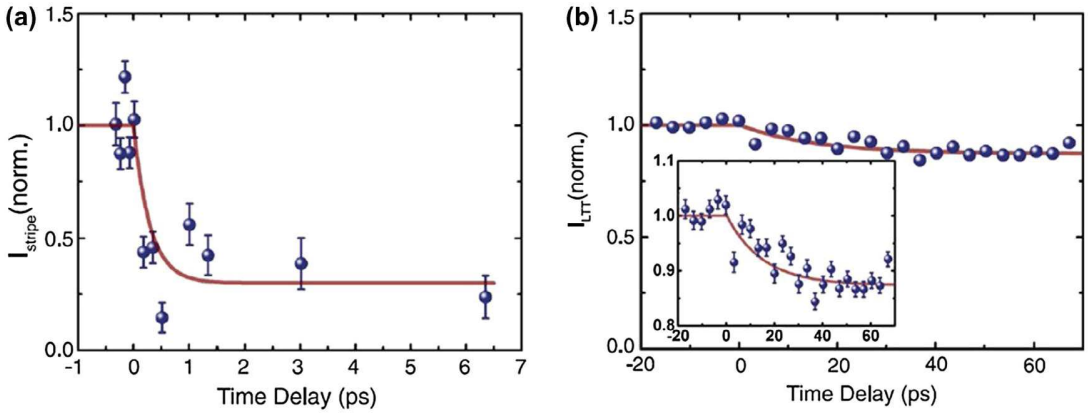

Figure 6. (a) Transient intensity of the charge stripe order diffraction peak in $La_{1.875}Ba_{0.125}CuO_4$ measured at the (0.24 0 0.5) wave vector. MIR excitation results in a prompt sub-ps decrease of the scattered intensity. The red solid line represents an exponential function with a time constant set to 300 fs, i.e. the resolution of the experiment. (b) Corresponding changes in the intensity of the (0 0 1) diffraction peak (reflecting the LTT distortion) in the same crystal under same excitation conditions. The red solid line is a single exponential fit to the data yielding a time constant of 15 ps.

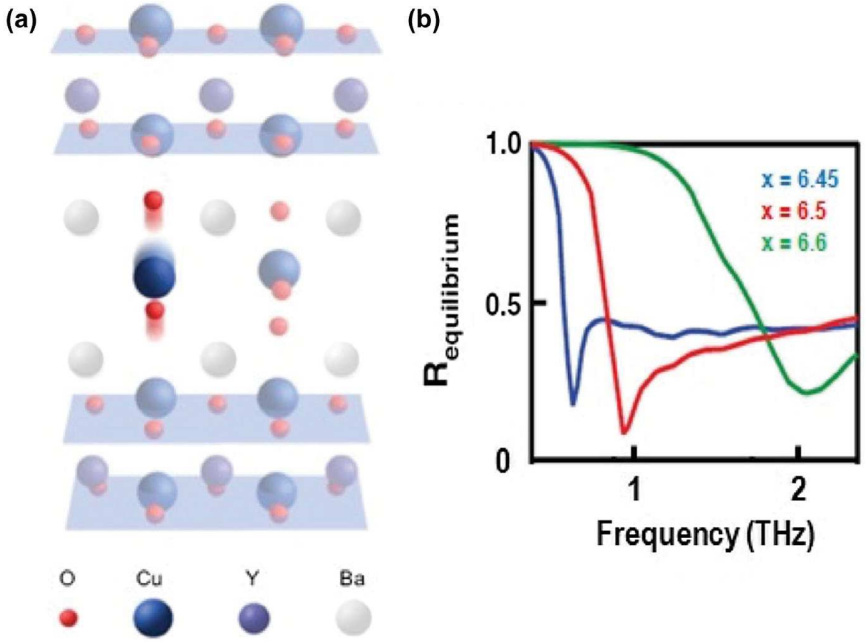

Figure 7. (a) Crystal structure of orthorhombic $YBa_2Cu_3O_{6.5}$ and sketch of the resonantly excited B_{1u}-symmetry IR-active phonon mode, comprising *c*-axis motions of the apical oxygen atoms between bilayers. (b) Equilibrium reflectivity spectra of $YBa_2Cu_3O_{6.45}$, $YBa_2Cu_3O_{6.5}$ and $YBa_2Cu_3O_{6.6}$ measured along the *c* axis, showing clear edges at the JPR frequencies.

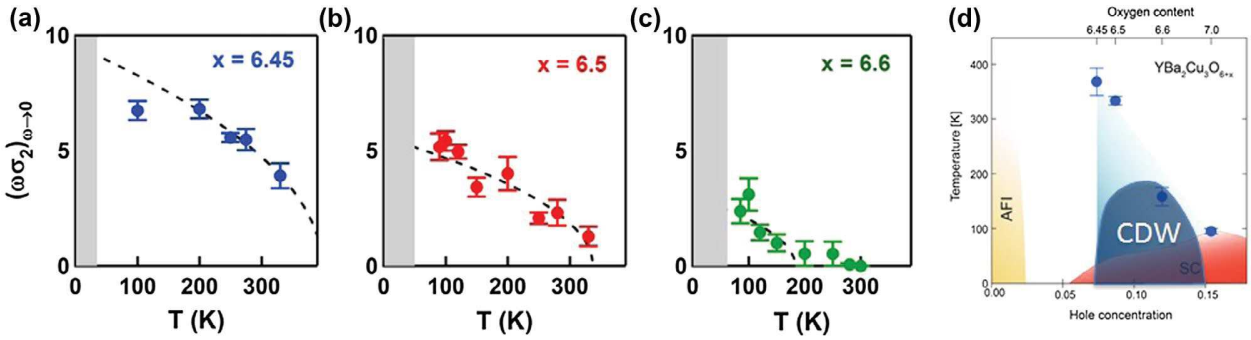

Figure 8. (a)–(c) Strength of the light-induced inter-bilayer coupling measured in $YBa_2Cu_3O_{6.45}$, $YBa_2Cu_3O_{6.5}$ and $YBa_2Cu_3O_{6.6}$ at +1-ps pump–probe delay as a function of base temperature and quantified by the zero-frequency extrapolation of the enhancement in imaginary conductivity. Grey-shaded regions refer to the equilibrium superconducting state. (d) Phase diagram of $YBa_2Cu_3O_x$. AFI, CDW and SC refer to the equilibrium antiferromagnetic insulating, charge density wave, and superconducting phase, respectively. The light blue shading represents the region where signatures of possible light-induced superconductivity were measured, delimited by the blue points, which were estimated from data in (a)–(c).

Even more strikingly, when the base temperature was raised to 100 K, i.e. above the highest equilibrium T_c of the $YBa_2Cu_3O_x$ family a light-induced reflectivity edge was measured at ~1-ps time delay after excitation. As for the equilibrium JPR (Figure 7(b)), this edge was located in the 1–2-THz frequency range and was found to stiffen with increasing hole doping.

A temperature scale T' for the disappearance of light-induced superconductivity ($\Delta\sigma_2 = 0$) was determined for each doping (see Figure 8(a)–(c)). T' was found to increase with decreasing hole concentration and to exceed room temperature at $x = 6.45$, with a trend very similar to the well-known 'pseudogap' transition line T^* [56] (see phase diagram in Figure 8(d)).

The pseudogap phase in the equilibrium phase diagram of high-T_c cuprates defines a region ($T < T^*$) characterised by highly anomalous electronic properties, where the possible presence of pre-formed Cooper pairs without phase coherence has been discussed in the past [42,57,58]. The experimental observations reported above could thus

suggest that phonon excitation may act on preformed pairs and transfer phase coherence to them, giving rise to a transient superconductor.

A second Josephson plasmon for these bilayer materials was also analysed. This mode is located around ~15 THz and is related to the Josephson tunnelling within the bilayer units of the $YBa_2Cu_3O_x$ crystal structure [59,60] (see Figure 8(a)). Like the low-frequency JPR, also the intra-bilayer one appears as an edge in reflectivity or as a peak in the loss function, and, additionally, the presence pf two 'acoustic' plasmons between and within the bilayers gives rise to a third 'optical' plasma mode (so-called transverse JPR). This mode appears as a peak in the real part of the optical conductivity, $\sigma_1(\omega)$ (Figure 8(b)).

At equilibrium, the intra-bilayer JPR is observed at temperatures much higher than T_c (up to ~150 K) and its presence has been utilised to define a region of the $YBa_2Cu_3O_x$ phase diagram with precursors of superconductivity in the normal state, possibly characterised by coherent tunnelling of preformed Cooper pairs within the bilayer units [61,62].

Time-resolved ultrabroadband (1–15 THz) spectroscopy at x = 6.5 doping ($YBa_2Cu_3O_{6.5}$) revealed crucial details of the microscopic physics. The transient optical properties of be well fitted at all temperatures and time delays by assuming an effective medium with two components: the first one (≳80%) was substantially not affected by MIR excitation, while the second, photo-susceptible one (≲20%) showed a blue-shifted (photo-induced) low-frequency JPR below (above) T_c, concurrently with a red-shifted intra-bilayer plasmon. Representative results of these fits are reported in Figure 9(c)–(d).

All the observations above point to a scenario in which inter-bilayer Josephson coupling is enhanced (or induced) at the expenses of the intra-bilayer tunnelling strength, while the number of Cooper pairs stays constant. This redistribution of coherent coupling takes place only in a fraction (≲20%) of the material, throughout the pseudogap phase $YBa_2Cu_3O_{6+x}$.

In search for a microscopic picture for the exotic dynamics observed in $YBa_2Cu_3O_x$ after MIR excitation, the non-linear lattice dynamics was investigated in the x = 6.5 sample using femtosecond hard X-ray diffraction at the LCLS free electron laser. Referring back to the discussion on non-linear lattice dynamics discussed above, we see by elementary group theory that the resonantly driven B_{1u} phonon mode can only couple to Raman-active phonons of A_g symmetry, because the direct product $B_{1u} \otimes B_{1u}$ is of A_g symmetry. By means of density functional theory calculations four strongly coupled A_g Raman modes were identified, all involving c-axis motion of the apical oxygen and planar copper atoms. According to the theory of non-linear phononics, the crystal lattice is then promptly distorted into a non-equilibrium structure along the linear combination of the atomic motions associated with these Raman modes.

In Figure 10(a), we report a measurement of non-linear lattice dynamics occurring in the transient superconducting state of $YBa_2Cu_3O_{6.5}$. Hard X-ray diffraction data were taken at 100 K, and gave rise to coherent inter-bilayer

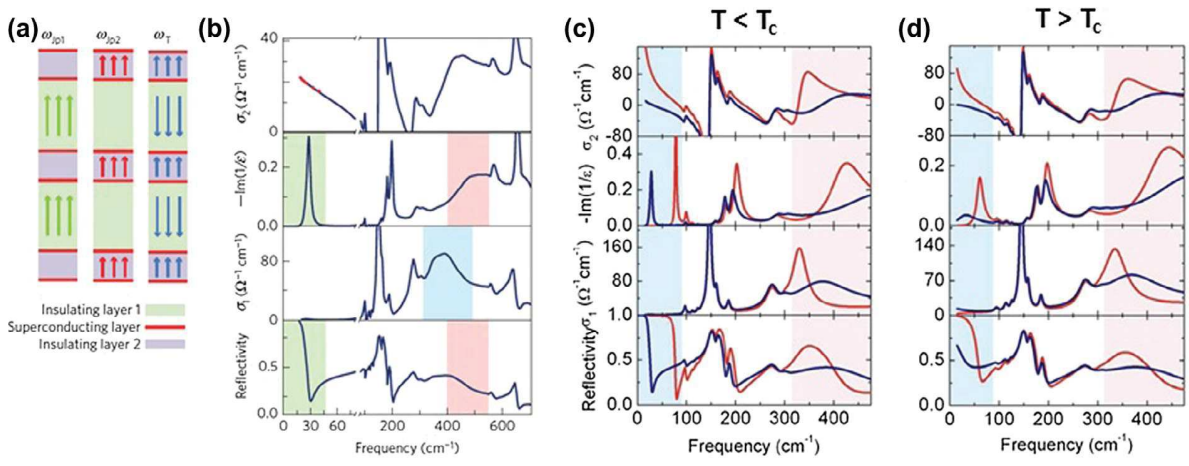

Figure 9. (a) In the superconducting state, the structure of $YBa_2Cu_3O_{6.5}$ can be viewed as two Josephson junctions in series, which gives rise to two longitudinal modes (ω_{Jp1}, ω_{Jp2}) and a transverse mode (ω_T) (arrows indicate the direction of the current). (b) Equilibrium c-axis optical properties of $YBa_2Cu_3O_{6.5}$. Superconductivity is evidenced by the $1/\omega$ divergence (red dashed) in the imaginary conductivity. Two longitudinal JPRs appear as peaks in the loss function and edges in reflectivity (green and red shaded). The transverse JPR appears as a peak in σ_1 (blue shaded). (c)–(d) Effective medium fits used to reproduce the transient broadband optical response after MIR excitation. Blue curves refer to the unperturbed component (≳80%) (equilibrium superconductor below T_c and normal insulator above T_c). Red curves indicate the photo-susceptible component (≲20%), which has a stiffer inter-bilayer JPR and red-shifted high-frequency plasmons. Frequency is shown here in cm^{-1} (1 THz = 33 cm^{-1}).

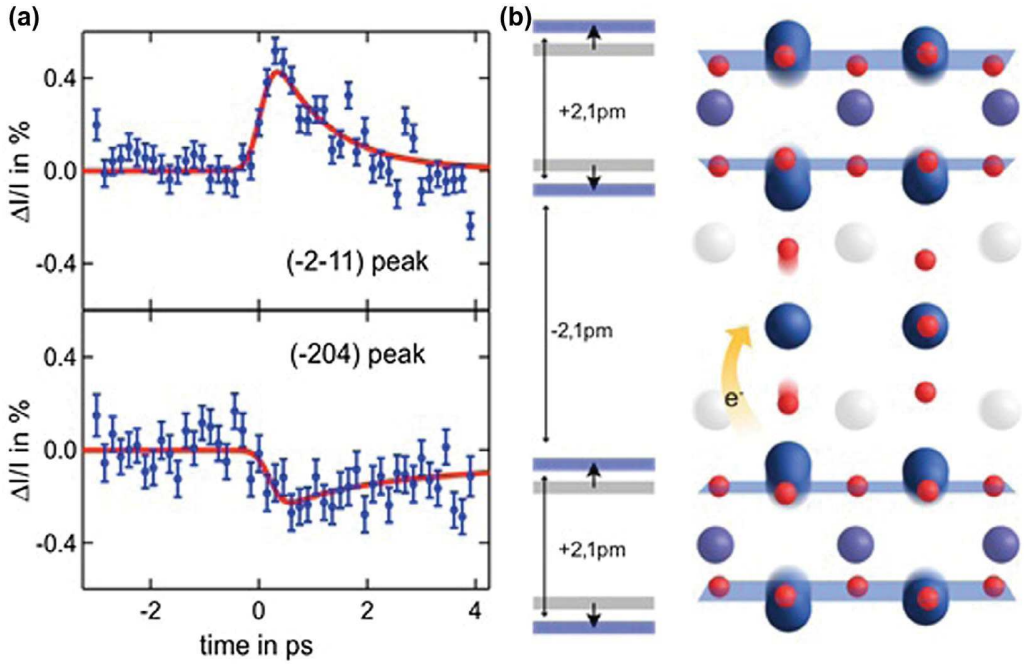

Figure 10. (a) Relative changes in diffracted intensity of the (−2 −1 −1) and the (−2 0 4) Bragg peaks measured in $YBa_2Cu_3O_{6.5}$ after MIR excitation at 100 K. Results of simultaneous fits to all data are shown as red lines. (b) Sketch of the reconstructed transient crystal structure at the peak signal. The atomic displacements from the equilibrium structure involve a decrease in inter-bilayer distance, accompanied by an increase in intra-bilayer distance.

transport. The dynamics of two representative diffraction peaks, the (−2 −1 1) and (−2 0 4), are displayed. A prompt change in diffracted intensity was observed, as expected from the rearrangement of the atoms in the unit cell predicted by the model of non-linear phonics. The decay to the equilibrium structure happened on the same timescale as the relaxation of light-induced superconductivity, indicating an intimate connection.

The exact amplitude and sign of the changes in diffraction intensity carry fundamental information on the light-induced lattice rearrangement. In order to reconstruct the transient crystal structure, the computed coupling strengths to the A_g Raman modes were combined with structure factor calculations, predicting the changes in diffraction intensity of all measured Bragg peaks for any given B_{1u} amplitude. The dynamics of all measured Bragg peaks could then be fitted simultaneously with the driving amplitude as only free parameter (fits shown as red curves in Figure 10(a)).

The reconstructed transient crystal structure of Figure 10(b) shows an increase in the in-plane O–Cu–O bond buckling and a decrease in apical oxygen to planar copper distance. Furthermore, the intra-bilayer distance increases, whereas the CuO_2 planes within the bilayers move closer together, effectively enhancing the inter-bilayer coupling. This last observation is intuitively consistent with the ultrabroadband THz spectroscopy measurements reported in Section 3.2, which indicated that the appearance of inter-bilayer superconducting coupling comes at the expenses of intra-bilayer tunnelling strength.

Density functional theory calculations using the transient crystal structure predict also a charge transfer from the CuO_2 planes to the Cu–O chains, effectively increasing the hole doping of the planes. Such self-doping effect was recently found to accompany the temperature-driven superconducting transition at equilibrium in $YBa_2Cu_3O_{6.9}$ and might be of key importance to explain the formation of the superconducting phase [63].

The non-linear lattice dynamics described above is expected not only to induce a directional displacement in the crystal lattice along all coupled Raman mode coordinates. The theory of non-linear phononics (see Section 2) predicts in addition that all displaced modes which have a long period compared to the excitation pulse duration will exhibit coherent oscillations about the displaced atomic positions. The coherent lattice response of $YBa_2Cu_3O_{6.55}$ was measured using an optical probe, in order to provide a complete picture of the structural dynamics in the light-induced superconducting state [64].

Atomic motions along Raman mode coordinates modulate the polarizability tensor and can be observed as an oscillation in the sample reflectivity. Therefore, this coherent structural response was measured by probing the transient reflectivity using 35-fs pulses at 800-nm wavelength.

MIR pulses were used to resonantly excite the IR-active B_{1u} mode. Under these conditions, all A_g Raman modes with finite coupling to the B_{1u} mode of up to ~6 THz in frequency are expected to be coherently driven.

Oscillations in the transient reflectivity were found by probing both in the *ab* and *c* directions, as shown in Figure 11(a). Three dominant frequency components appeared in the Fourier transform spectrum, attributed to the four lowest frequency A_g modes of $YBa_2Cu_3O_{6.55}$ (Figure 10(b)). Consistent with the Raman tensor for the A_g modes, the phase of the coherent response was the same for the two orthogonal probe polarisations [65].

The oscillation amplitudes in real space could not be quantified from these data alone, as the changes in the 800-nm polarizability depend on the unknown Raman tensor elements [66]. However, an estimate of the oscillatory amplitude could be obtained by combining these data with the previous X-ray diffraction experiment. According to this analysis, the coherent atomic motion is dominated by a change in distance of planar Cu atoms *d* along the crystallographic *c* axis, as sketched in Figure 11(c). Following excitation, the Cu atoms of bilayers move apart from each other by ~3 pm, corresponding to a relative change in distance of 1%. This motion is accompanied by coherent oscillations with an estimated amplitude of ~0.9 pm, which decay within 3 ps after excitation (see Figure 11(d)).

According to the density functional theory calculations [62], this oscillatory motion would induce periodic charge redistributions between the Cu atoms of planes and chains, which may cause a dynamical stabilisation of interlayer fluctuations by a modulation of electronic properties [67].

4. Photo-induced superconductivity in K_3C_{60}

Similar excitation of vibrational modes was applied more recently to K_3C_{60}, a molecular solid in which superconductivity at equilibrium below T_c = 20 K [68], mediated by a combination of electronic correlations [69] and local molecular vibrations [70]. K_3C_{60} crystallises in a face-centred cubic structure (Figure 12(a)), where each C_{60}^{3-} ion contributes three half-filled t_{1u} molecular orbitals to form narrow bands [71] (see Figure 11)

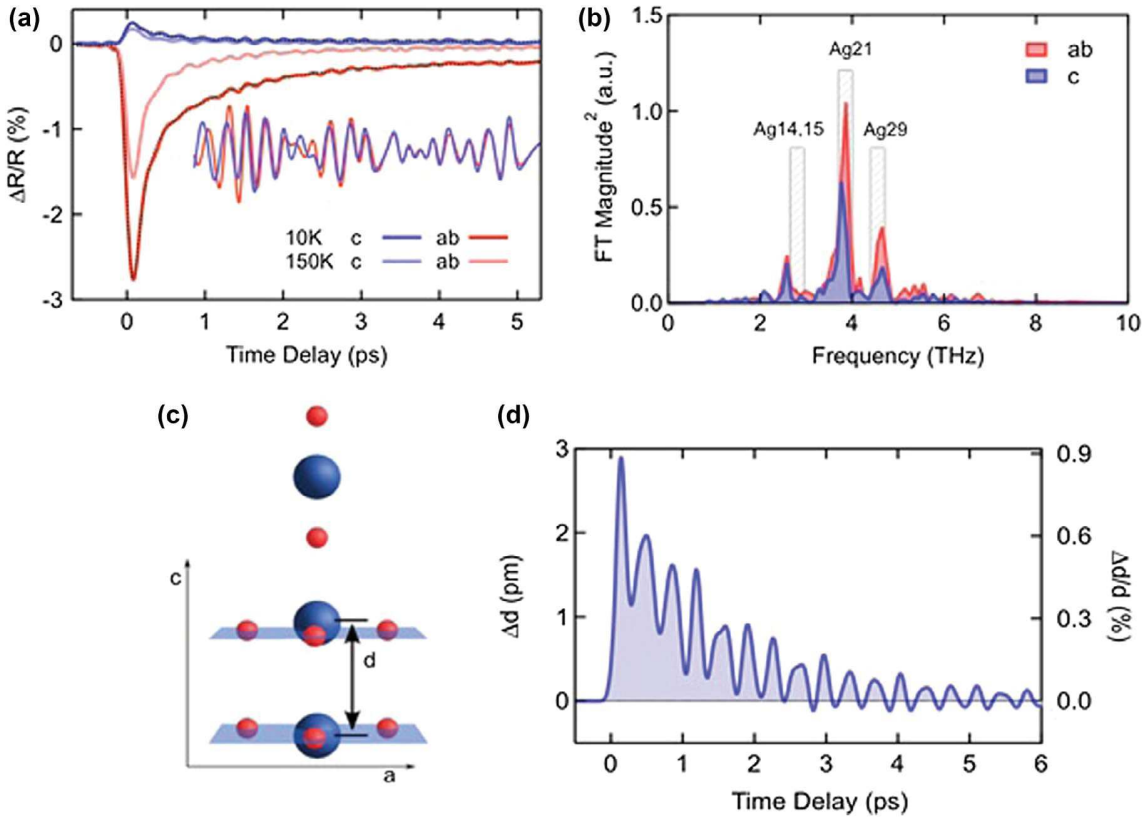

Figure 11. (a) Time-resolved changes in the reflection of 800-nm pulses polarised in-plane (*ab*) and out-of-plane (*c*) following MIR excitation. The oscillatory components shown in the inset are extracted from the 10 K measurement. (b) Fourier transform of these oscillations, showing three components, attributed to four different A_g Raman modes. (c) Combined atomic motion of the A_g modes, which mainly involves *c*-axis movement of the planar Cu atoms. *d* is here the distance between Cu atoms of neighbouring CuO_2. (d) Calculated changes in *d*, including the full structural dynamics composed of displacive and oscillatory response.

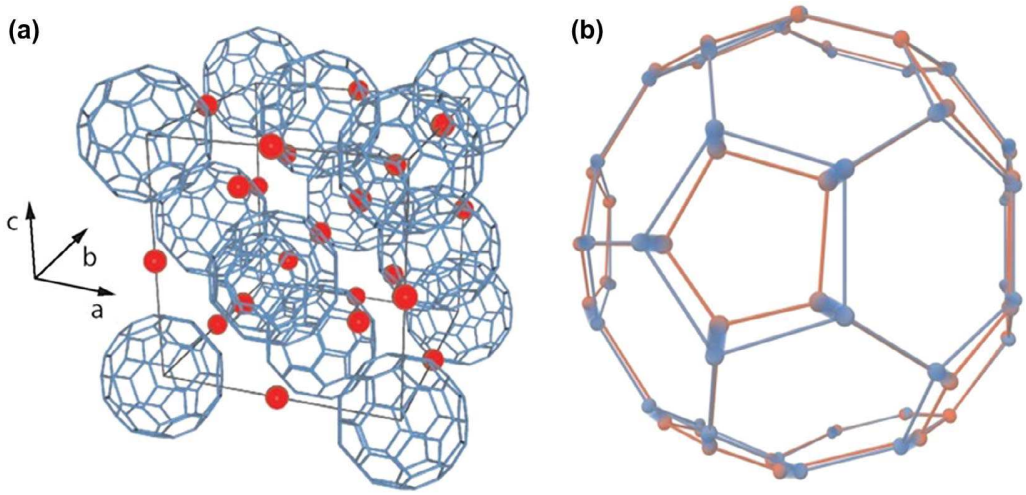

Figure 12. (a) Face-centred cubic unit cell of K_3C_{60}. Blue bonds link the C atoms on each C_{60} molecule. K atoms are represented as red spheres. (b) C_{60} molecular distortion (red) along the T_{1u} vibrational mode coordinates. The equilibrium structure is displayed in blue.

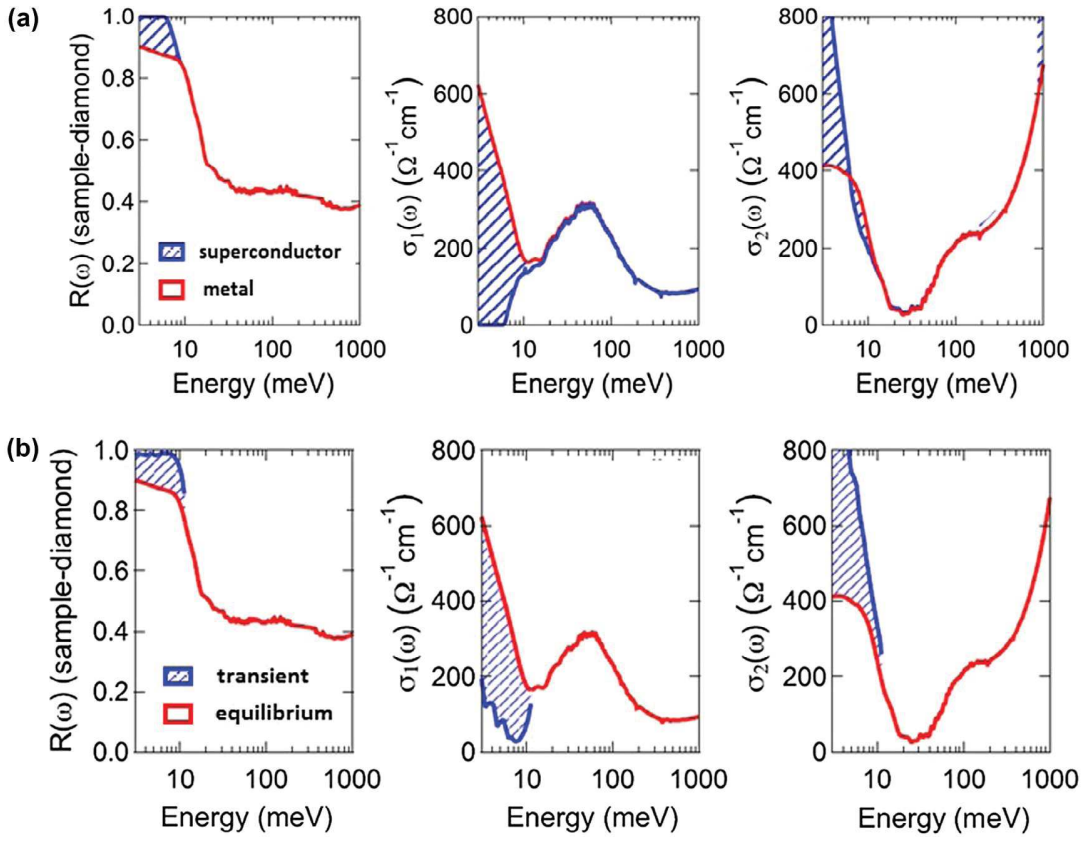

Figure 13. (a) Equilibrium reflectivity and complex optical conductivity of K_3C_{60} measured at $T = 25$ K (red) and $T = 10$ K (blue). (b) Same quantities measured at a base temperatures $T = 25$ K at equilibrium (red) and 1 ps after MIR excitation (blue).

In our experiments, femtosecond MIR pulses were tuned between 6 and 15 μm (a spectral region where different local molecular vibrations are present) and used to excite K_3C_{60}. The resulting changes in THz frequency reflectivity and optical conductivity were determined at different pump–probe time delays and normalised to the absolute equilibrium optical properties measured on the same sample.

In Figure 13, we show the transient response (reflectivity and complex conductivity) measured in metallic K_3C_{60} at high temperature after MIR excitation at 7 μm (resonant with the T_{1u} molecular mode displayed in Figure 12(b)), along with the superconducting response measured at equilibrium below T_c.

For all temperatures between $T_c = 20$ K and $T = 100$ K, photoexcitation-induced transient changes in the optical properties very similar to those observed when cooling at equilibrium: at 1-ps pump–probe time delay, a saturated reflectivity at $R = 1$, a gapped $\sigma_1(\omega)$, and divergent $\sigma_2(\omega)$ were observed. Furthermore, all transient optical spectra could be fitted with the same function used for the low-temperature superconductor at equilibrium.

The non-equilibrium fits evidenced a gap in the non-equilibrium $\sigma_1(\omega)$ nearly twice as large as the superconducting gap at equilibrium. When the same experiment was repeated at higher base temperatures, the effect progressively disappeared, although a sizeable enhancement in carrier mobility could be measured up to room temperature.

These data indicate that excitation of molecular vibrations can coherently stimulate a transition from the high-temperature metallic state into a non-equilibrium superconducting phase. For the strong optical fields used in the experiment (~1.5 MV/cm) and from the polarizability of the T_{1u} molecular vibrations, one can estimate large oscillatory distortions of the C–C bonds amounting to several per cents of their equilibrium bond lengths. Hence, in analogy with the non-linear phononics scenario introduced above, the large amplitude excitation is expected to extend beyond linear response and to deform the structure of the solid along other, anharmonically coupled coordinates.

To lowest order, these couplings are described by $q^2_{T_{1u}} Q$ terms in the nonlinear lattice Hamiltonian, where $q_{T_{1u}}$ is the directly driven mode coordinate, and Q is the coordinate of any distortion contained in the irreducible representation of $T_{1u} \times T_{1u}$. A sizeable distortion is expected along normal mode coordinates of H_g symmetry. Because H_g modes are thought to assist pairing at equilibrium [71], it is possible that a quasi-static H_g molecular deformation might favour stronger superconductivity, for example, by causing an increase in the electron–phonon coupling.

Excitation of local T_{1u} vibrations is also expected to modulate local electronic correlations. An order-of-magnitude estimate for this effect has been extracted from frozen atomic motions for the T_{1u} mode, predicting an increase in U as high as ~10% for the orbitals orthogonal to the vibration. Such large asymmetric change would unbalance the occupancy of the three t_{1u} orbitals and possibly interplay with the dynamical Jahn–Teller coupling, which is known to contribute to superconductivity near equilibrium [72].

5. Theories of photo-induced superconductivity

The first attempt to describe the phenomena above has followed the idea of light induced melting of a competing charge order, which is expected to enhance superconductivity. This may well apply to the single layer cuprates and to the bilayers, although probably only close to 1/8 doping (e.g. $YBa_2Cu_3O_{6.6}$). Specifically, these studies have analysed the role of apical oxygen excitation discussed in Section 3.

A Floquet expansion for a time modulated apical oxygen [73] shows how the exponentially dependent interlayer tunnelling $t_z = Ae^{-d}$ is modified on average. If the distance $d(t)$ is both displaced and modulated with a zero average optical field $d(t) = d_0 + \Delta d_1 + \Delta d_2 \sin \omega t$, two effects appear. Firstly, a quasi-static Δd_1 brings the layers closer to one another on average. Secondly, a periodic modulation $\Delta d_2 \sin \omega t$ factors into the exponential z-axis tunnelling as $t_z = Ae^{-d+\Delta d_2 \sin \omega t}$, and provides an additional enhancement on average. An increase in the T_c by even 100% was predicted, along with a suppression of charge order due to a change in nesting conditions, also consistent with the experimental observations.

In the same context, the use of a laser to affect the competition between superconductivity (SC) and a charge density wave (CDW) was studied in the Hubbard model in Ref. [74]. It was shown that a light-field interacts with the SC and CDW orders differently, and hence affects their competition in a frequency-dependent fashion. Remarkably, it was shown that optical excitation can favour either CDW order or SC order depending on whether the light is tuned to the red or to the blue of the equilibrium single-particle energy gap, respectively. It has not been possible yet to test these ideas as the non-linear THz pumps are only partially tuneable, although recent developments in optical technology and the development of new optical sources at THz frequencies will make these experiments feasible [75].

Similarly, the effect of lattice excitation on the competition between CDW and SC was analysed [76] in the context of bond density wave order in the cuprates. In this case, fourth-order non-linear phonics was considered, and especially the possibility of driving pairs of phonons at opposite momenta ($\pm k$), which possess high density of states because of the Bond Density Wave induced softening. Quartic coupling of this type has been considered also in other contexts [77], in which it was shown that coherent excitation of pairs of phonons at opposite momenta ($\pm k$) could in fact drive squeezed vibrational motion, and, provided that dissipation and heating would not destroy coherence [78], parametrically amplify the superconducting instability. In a related context, dynamical enhancement was considered as an effect of a parametric term

on the BCS wavefunction [79] or as a means to enhance superexchange pairing in the Hubbard model [80].

Other imaginative approaches to explain this class of phenomena have also introduced other, genuinely dynamical processes. Several papers have considered the effect that the excitation and the time-dependent modulation on the spectrum of phase fluctuations that reduce superconductivity in the strong coupling limit. For example, such modulations were shown to 'cool' phase fluctuations for specific pump frequencies [81, 82] and, most recently, the possibility of either reducing or amplifying these fluctuations in similar conditions [72, 83–85].

Kennes et al. [86] have approached the problem specifically in the context of the K_3C_{60} experiments of Section 4. This paper starts from the analysis of a strongly excited molecular site in each C_{60}^{3-} unit. The paper is especially interesting as it considers a situation in which electronic squeezing for these molecules is large, that is, vibrational levels renormalise strongly when the charge state of the molecule is changed. In this situation, when high vibrational occupation is achieved by a light field, the squeezing provides an energy gain when the molecule is doubly occupied, one in which Coulomb repulsion can be overcome and hence creating attraction and pairing. Similar phenomena were discussed experimentally for one-dimensional Mott insulators like ET-F_2TCNQ [87, 88].

More comprehensive analyses of the specific physics of K_3C_{60} was reported by Kim et al. [89] and by Mazza and Georges [90], who computed static and dynamical changes in the threefold degenerate orbital structure of the C_{60}^{3-} and especially the orbital dependence of the Coulomb repulsion in a distorted state. Considering quasi-static distortions along the driven mode coordinate, Kim and co-workers found that the orbitally selective interaction degeneracy was lifted by the optical stimulation. It was argued in this paper that under these conditions only two orbitals of the molecule participate in the pairing and that T_c can be increased as a consequence of the increase in fluctuations.

Many other papers, which will not be discussed in further detail, have considered related mechanisms, typically starting from a quench of either kinetic energy [91] or interactions [92], to provide enhancement or appearance of a previously week or absent superconducting state.

6. Concluding remarks

We have discussed how selective excitation of specific vibrational modes and the non-linear response of the lattice can drive striking non-equilibrium emergent properties of solids, and, in fact, create superconducting like coherence or non-equilibrium fluctuations at previously unimaginable temperatures. Looking forward, one foresees advances in these areas of research.

Fuelled by a staggering technological revolution in laser techniques, optical methods at short timescales have now conquered the entire electromagnetic spectrum, covering continuously all frequency scales from microwaves to X-rays. X-ray-free electron lasers are only one of the striking new developments in this area and one that promises new, important materials research. In an effort that we can term *non-equilibrium materials discovery*, the discovery of new functionalities at short timescales, and the use of free electron lasers to measure the transient crystal structures, could inspire materials design directions to stabilise these deformations enhanced characteristics.

Also, the discovery of light induced superconductivity in unconventional materials like the cuprates and the doped fullerenes seems to inspire a growing number of researchers. The effect is not understood, although the many theoretical approaches seem to underscore how modulation at specific frequencies can be used to extend quantum coherence in a solid. This is perhaps not too surprising when one considers the many forms of synchronisation between arrays of oscillators by periodic driving. The possibility of creating room temperature superconductors powered by light is indeed a great dream of the author, and one that is inspiring intense activity. A sobering remark in this context starts form the realisation that the electric fields necessary to induce such coherences still exceeds 1 MV/cm and the peak powers of the femtosecond pulses used are in the MW range. These phenomena are so far inherently transient, not only because it is difficult to create longer pulses at these field strengths but also because heating is expected to make stabilisation unrealistic. However, a precise understanding of the microscopic physics may open up orders of magnitude gains in efficiency, providing new schemes that make use of efficient coupling of light into the appropriate microscopic degrees of freedom.

Disclosure statement

No potential conflict of interest was reported by the author.

Notes on contributor

Andrea Cavalleri has been a professor of Physics at the University of Oxford since 2006, having served in the same faculty as a university lecturer between 2005 and 2006. Since 2008, he has also been the founding director for the Max Planck Institute for the Structure and Dynamics of Matter. Before joining the Oxford faculty, Cavalleri was a visiting student, a postdoctoral appointee and a staff scientist at the University of Essen (Germany) at the University of California,

San Diego and at the Lawrence Berkeley National Laboratory, respectively. He is best known for his work on the control of non-equilibrium phenomena in quantum solids, and most recently with his demonstration of photo-induced superconductivity in high T_c cuprates and in doped fullerites. Cavalleri has been recognised with several awards, including the 2004 European Young Investigator Award, the Max Born Medal from the Institute of Physics and the German Physical Society (2015), the Dannie Heinemann Prize from the Academy of Sciences in Goettingen (2015) and the Frank Isakson Prize from the American Physical Society. He is also a recipient of one of the first ERC Synergy Grants. Cavalleri is a fellow of the APS, of the AAAs, and of the IoP. In 2017, he was elected to be a Member of the Academia Europaea.

References

[1] Fiebig M, Miyano K, Tomioka Y, et al. Visualization and switching of the local insulator–metal transition in $Pr_{0.7}Ca_{0.3}MnO_3$. Science. 1998;280:1925.

[2] Cavalleri A, Toth C, Siders CW. Femtosecond structural dynamics in VO_2 during a solid-to-solid phase transition. Phys Rev Lett. 2001;87:237401.

[3] Cavalleri A, Rini M, Chong HHW, et al. Band-selective measurements of electron dynamics in VO_2 using femtosecond near-edge X-ray absorption. Phys Rev Lett. 2005;95:067405.

[4] Okamoto H, Matsuzaki H, Wakabayashi T, et al. Photoinduced metallic state mediated by spin-charge separation in a one-dimensional organic Mott insulator. Phys Rev Lett. 2007;98:037401.

[5] Wall S, Brida D, Clark SR, et al. Quantum interference between charge excitation paths in a solid-state Mott insulator. Nat Phys. 2011;7:114–118.

[6] Uemura H, Matsuzaki H, Takahashi Y, et al. Ultrafast charge dynamics in organic one-dimensional Mott insulators. Phys B. 2010;405:S357–S359.

[7] Ehrke H, Tobey RI, Wall S, et al. Photoinduced melting of antiferromagnetic order in $La_{0.5}Sr_{1.5}MnO_4$ measured using ultrafast resonant soft X-ray diffraction. Phys Rev Lett. 2011;106:217401.

[8] Polli D, Rini M, Wall S, et al. Coherent orbital waves in the photo-induced insulator–metal dynamics of a magnetoresistive manganite. Nat Mater. 2007;6:643–647.

[9] Allen PB. Theory of thermal relaxation of electrons in metals. Phys Rev Lett. 1987;59:1460–1463.

[10] Fann WS, Storz R, Tom HWK, et al. Direct measurement of nonequilibrium electron-energy distributions in subpicosecond laser-heated gold films. Phys Rev Lett. 1992;68:2834–2837.

[11] Hoffmann MC, Fülöp JA. Intense ultrashort terahertz pulses: generation and applications. J Phys D Appl Phys. 2011;44:083001.

[12] Nicoletti D, Cavalleri A. Nonlinear light matter interactions at terahertz frequencies. Adv Opt Phot. 2016;8:401–464.

[13] Wallis RF, Maradudin AA. Ionic Raman effect. II. The first-order ionic Raman effect. Phys Rev B. 1971;3:2063–2075.

[14] Martin TP, Genzel L. Ionic Raman scattering and ionic frequency mixing. Phys Status Solidi B. 1974;61:493–502.

[15] Mills DL. Ionic contributions to the Raman tensor of insulators. Phys Rev B. 1987;35:9278–9283.

[16] Först M, Manzoni C, Kaiser S, et al. Nonlinear phononics as an ultrafast route to lattice control. Nat Phys. 2011;7:854–856.

[17] Först M, Mankowsky R, Bromberger H, et al. Displacive lattice excitation through nonlinear phononics viewed by femtosecond X-ray diffraction. Solid State Commun. 2013;169:24–27.

[18] Mankowsky R, von Hoegen A, Först M, et al. Ultrafast reversal of the ferroelectric polarization. Phys Rev Lett. 2017;118:197601.

[19] Rini M, Tobey R, Dean N, et al. Control of the electronic phase of a manganite by mode-selective vibrational excitation. Nature. 2007;449:72–74.

[20] Tobey RI, Prabhakaran D, Boothroyd AT, et al. Ultrafast electronic phase transition in $La_{1/2}Sr_{3/2}MnO_4$ by coherent vibrational excitation: evidence for non-thermal melting of orbital order. Phys Rev Lett. 2008;101:197404.

[21] Först M, Tobey R, Wall S, et al. Driving magnetic order in a manganite by ultrafast lattice excitation. Phys Rev B. 2011;84:241104.

[22] Bednorz JG, Mueller KA. Possible high T_c superconductivity in the Ba–La–Cu–O system. Z Phys B. 1986;64:189–193.

[23] Anderson PW. The resonating valence bond state in La_2CuO_4 and superconductivity. Science. 1987;235:1196–1198.

[24] Zaanen J, Gunnarsson O. Charged magnetic domain lines and the magnetism of high-T_c oxides. Phys Rev B. 1989;40:7391–7394.

[25] Tranquada J, Sternlieb BJ, Axe JD, et al. Evidence for stripe correlations of spins and holes in copper oxide superconductors. Nature. 1995;375:561–563.

[26] Moodenbaugh AR, Xu Y, Suenaga M, et al. Superconducting properties of $La_{2-x}Ba_xCuO_4$. Phys Rev B. 1998;38:4596–4660.

[27] Hücker M, von Zimmermann M, Gu GD, et al. Stripe order in superconducting $La_{2-x}Ba_xCuO_4$ (0. 095≤x≤0.155). Phys Rev B. 2011;83:104506.

[28] Suzuki T, Fujita T. Low-temperature crystalline structure of $(La_{1-x}Ba_x)_2CuO_{4-\delta}$. Phys C. 1989;159:111–116.

[29] Crawford MK, Harlow RL, McCarron EM, et al. Lattice instabilities and the effect of copper-oxygen-sheet distortions on superconductivity in doped La_2CuO_4. Phys Rev B. 1991;44:7749–7752.

[30] Fujita M, Goka H, Yamada K, et al. Competition between charge- and spin-density-wave order and superconductivity in $La_{1.875}Ba_{0.125-x}Sr_xCuO_4$. Phys Rev Lett. 2002;88:167008.

[31] Fink J, Schierle E, Weschke E, et al. Charge ordering in $La_{1.8-x}Eu_{0.2}Sr_xCuO_4$ studied by resonant soft X-ray diffraction. Phys Rev B. 2009;79:100502.

[32] Fink J, Soltwisch V, Geck J, et al. Phase diagram of charge order in $La_{1.8-x}Eu_{0.2}Sr_xCuO_4$ from resonant soft X-ray diffraction. Phys Rev B. 2011;83:092503.

[33] Klauss H-H, Wagener W, Hillberg M, et al. From antiferromagnetic order to static magnetic stripes: The phase diagram of $(La,Eu)_{2-x}Sr_xCuO_4$. Phys Rev Lett. 2000;85:4590–4593.

[34] Suryadijaya LP, Sasakawa T, Takagi H. Oxygen isotope effect on charge/spin stripes in $La_{1.8-x}Eu_{0.2}Sr_xCuO_4$. Phys C. 2005;426–431:402.

[35] Takeshita N, Sasagawa T, Sugioka T, et al. Gigantic anisotropic uniaxial pressure effect on superconductivity within the CuO_2 plane of $La_{1.64}Eu_{0.2}Sr_{0.16}CuO_4$: strain control of stripe criticality. J Phys Soc Jpn. 2004;73:1123–1126.

[36] Hücker M, von Zimmermann M, Debessai M, et al. Spontaneous symmetry breaking by charge stripes in the high pressure phase of superconducting $La_{1.875}Ba_{0.125}CuO_4$. Phys Rev Lett. 2010;104:057004.

[37] Thampy V, Dean MPM, Christensen NB, et al. Rotated stripe order and its competition with superconductivity in $La_{1.88}Sr_{0.12}CuO_4$. Phys Rev B. 2014;90:100510(R).

[38] Li Q, Hücker M, Gu GD, et al. Two-Dimensional superconducting fluctuations in stripe-ordered $La_{1.875}Ba_{0.125}CuO_4$. Phys Rev Lett. 2007;99:067001.

[39] Berg E, Fradkin E, Kim E-A, et al. Dynamical layer decoupling in a stripe-ordered high-T_c superconductor. Phys Rev Lett. 2007;99:127003.

[40] Rajasekaran S, Okamoto J, Mathey L, et al. Probing opticaly silent superfluid stripes in cuprates. arXiv: 1705.06112.

[41] Uemura YJ, Luke GM, Sternlieb BJ, et al. Universal correlations between T_c and $n_s/m*$ (carrier density over effective mass) in high-Tc cuprate superconductors. Phys Rev Lett. 1989;62:2317–2320.

[42] Emery VJ, Kivelson SA. Importance of phase fluctuations in superconductors with small superfluid density. Nature. 1995;374:434–437.

[43] Fausti D, Tobey RI, Dean N, et al. Light-induced superconductivity in a stripe-ordered cuprate. Science. 2011;331:189–191.

[44] Tamakasu K, Nakamura Y, Uchida S. Charge dynamics across the CuO_2 planes in $La_{2-x}Sr_xCuO_4$. Phys Rev Lett. 1992;69:1455.

[45] Kleiner R, Steinmeyer F, Kunkel G, et al. Intrinsic Josephson effects in $Bi_2Sr_2CaCu_2O_8$ single crystals. Phys Rev Lett. 1992;68:2394–2397.

[46] Basov DN, Timusk T, Dabrowski B, et al. c-Axis response of $YBa_2Cu_4O_8$: a pseudogap and possibility of Josephson coupling of CuO_2 planes. Phys Rev B. 1994;50:3511–3514.

[47] Tajima S, Noda T, Eisaki H, et al. c-Axis optical response in the static stripe ordered phase of the cuprates. Phys Rev Lett. 2001;86:500–503.

[48] Först M, Tobey RI, Bromberger H, et al. Melting of charge stripes in vibrationally driven $La_{1.875}Ba_{0.125}CuO_4$: assessing the respective roles of electronic and lattice order in frustrated superconductors. Phys Rev Lett. 2014;112:157002.

[49] Abbamonte P, Rusydi A, Smadici S, et al. Spatially modulated 'Mottness' in $La_{2-x}Ba_xCuO_4$. Nat. Phys. 2005;1:155–158.

[50] Wilkins SB, Dean MPM, Fink J, et al. Comparison of stripe modulations in $La_{1.875}Ba_{0.125}CuO_4$ and $La_{1.48}Nd_{0.4}Sr_{0.12}CuO_4$. Phys Rev B. 2011;84:195101.

[51] Dmitrienko V. Forbidden reflections due to anisotropic X-ray susceptibility of crystals. Acta Crystallogr Sect A. 1983;39:29–35.

[52] Homes CC, Hücker M, Li Q, et al. Determination of the optical properties of $La_{2-x}Ba_xCuO_4$ for several dopings, including the anomalous x=1/8 phase. Phys Rev B. 2012;85:134510.

[53] Pavarini E, Dasgupta I, Saha-Dasgupta T, et al. Band-structure trend in hole-doped cuprates and correlation with $T_{c,max}$. Phys Rev Lett. 2001;87:047003.

[54] Averitt RD, Rodriguez G, Lobad AI, et al. Nonequilibrium superconductivity and quasiparticle dynamics in $YBa_2Cu_3O_{7-\delta}$. Phys Rev B. 2001;63:140502(R).

[55] Pashkin A, Porer M, Beyer M, et al. Femtosecond response of quasiparticles and phonons in superconducting $YBa_2Cu_3O_{7-\delta}$ studied by wideband terahertz spectroscopy. Phys Rev Lett. 2010;105:067001.

[56] Timusk T, Statt B. The pseudogap in high temperature superconductors. Rep Prog Phys. 1999;62:61–122.

[57] Gomes KK, Pasupathy AN, Pushp A, et al. Visualizing pair formation on the atomic scale in the high-T_c superconductor $Bi_2Sr_2CaCu_2O_{8+\delta}$. Nature. 2007;447:569–572.

[58] Corson J, Mallozzi R, Orenstein J, et al. Vanishing of phase coherence in underdoped $Bi_2Sr_2CaCu_2O_{8+\delta}$. Nature. 1999;398:22–223.

[59] van der Marel D, Tsvetkov AA. Transverse-optical Josephson plasmons: equations of motion. Phys Rev B. 2001;64:024530.

[60] van der Marel D, Tsvetkov AA. Transverse optical plasmons in layered superconductors. Czech J Phys. 1996;46:3165.

[61] Dubroka A, Rössle M, Kim KW, et al. Evidence of a precursor superconducting phase at temperatures as high as 180 K in $RBa_2Cu_3O_{7-\delta}$ (R=Y,Gd,Eu) superconducting crystals from infrared spectroscopy. Phys Rev Lett. 2011;106:047006.

[62] Uykur E, Tanaka K, Masui T, et al. Persistence of the superconducting condensate far above the critical temperature of $YBa_2(Cu,Zn)_3O_y$ revealed by c-axis optical conductivity measurements for several Zn concentrations and carrier doping levels. Phys Rev Lett. 2014;112:127003.

[63] Magnuson M, Schmitt T, Strocov VN, et al. Self-doping processes between planes and chains in the metal-to-superconductor transition of $YBa_2Cu_3O_{6.9}$. Sci. Rep. 2014;4:7017.

[64] Mankowsky R, Först M, Loew T, et al. Coherent modulation of the $YBa_2Cu_3O_{6+}x$ atomic structure by displacive stimulated ionic Raman scattering. Phys Rev B. 2015;91:094308.

[65] Hayes W, Loudon R. Scattering of light by crystals. New York (NY): Wiley; 1978.

[66] Stevens TE, Kuhl J, Merlin R. Coherent phonon generation and the two stimulated Raman tensors. Phys Rev B. 2002;65:144304.

[67] Höppner R, Zhu B, Rexin T, et al. Redistribution of phase fluctuations in a periodically driven cuprate superconductor. Phys Rev B. 2015;91:104507.

[68] Hebard AF, Rosseinsky MJ, Haddon RC, et al. Superconductivity at 18 K in potassium-doped C60. Nature. 1991;350:600–601.

[69] Capone M, Fabrizio M, Castellani C, et al. Strongly correlated superconductivity. Science. 2002;296:2364–2366.

[70] Varma CM, Zaanen J, Raghavachari K. Superconductivity in the fullerenes. Science. 1991;254:989–992.

[71] Gunnarsson O. Alkali-doped fullerides: narrow-band solids with unusual properties. 1st ed. Singapore: World Scientific; 2004.
[72] Laplace Y, Cavalleri A. Josephson plasmonics in layered superconductors. Adv Phys X. 2017;1:387–411.
[73] Raines ZM, Stanev V, Galitski VM. Enhancement of superconductivity via periodic modulation in a three-dimensional model of cuprates. Phys Rev B. 2015;91:184506.
[74] Sentef MA, Tokuno A, Georges A, et al. Theory of laser-controlled competing superconducting and charge orders. Phys Rev Lett. 2017;118:087002.
[75] Liu B, Bromberger H, Cartella A, et al. Generation of narrowband, high-intensity, carrier-envelope phase stable pulses tunable between 4 and 18 THz. Opt Lett. 2017;42:129–131.
[76] Patel AA, Eberlein A. Light induced enhancement of superconductivity via melting of competing bond density wave order in underdoped cuprates. Phys Rev B. 2016;93:195139.
[77] Babadi M, Knap M, Martin I, et al. Theory of parametrically amplified electron-phonon superconductivity. Phys Rev B. 2017;96:014512.
[78] Murakami Y, Tsuji N, Eckstein M, et al. Nonequilibrium steady states and transient dynamics of conventional superconductors under phonon driving. Phys Rev B. 2017;96:045125.
[79] Komnik A, Thorwart M. BCS theory of driven superconductivity. Eur. Phys. J. 2016;89:380.
[80] Coulthard JR, Clark SR, Al-Assam S, et al. Enhancement of superexchange pairing in the periodically driven Hubbard model. Phys Rev B. 2017;96:085104.
[81] Denny SJ, Clark SR, Laplace Y, et al. Proposed parametric cooling of bilayer cuprate superconductors by terahertz excitation. Phys Rev Lett. 2015;114:137001.
[82] Höppner R, Zhu B, Rexin T, et al. Dynamical redistribution of phase fluctuations in bi-layer superconductors by periodic driving with an optical field. Phys Rev B. 2015;91:104507.
[83] Rajasekaran S, Casandruc E, Laplace Y, et al. Parametric amplification of a superconducting plasma wave. Nat Phys. 2016;12:1012–1016.
[84] Okamoto J, Cavalleri A, Mathey L. Theory of enhanced interlayer tunneling in optically driven high Tc superconductors. Phys Rev Lett. 2016;117:227001.
[85] Okamoto J, Hu W, Cavalleri A, et al. Transiently enhanced interlayer tunneling in optically driven High T_c superconductors. arXiv: 1706.04554.
[86] Kennes D, Wilner E, Reichman DR, et al. Transient superconductivity from electronic squeezing of optically pumped phonons. Nat Phys. 2017;13:479–483.
[87] Kaiser S, Clark S, Nicoletti D, et al. Optical properties of a vibrationally modulated solid-state Mott insulator. Sci Rep. 2014;4:3823.
[88] Singla R, Cotugno G, Kaiser S, et al. THz-frequency modulation of the Hubbard U in an organic Mott insulator. Phys Rev Lett. 2015;115:187401.
[89] Kim MJ, Nomura Y, Ferrero M, et al. Enhancing superconductivity in A_3C_{60} fullerides. Phys Rev B. 2016;94:155152.
[90] Mazza G, Georges A. Non-equilibrium superconductivity in driven alkali-doped fullerites. arXiv: 17026.14675; 2017.
[91] Sentef M, Kemper AF, Georges A, et al. Theory of light enhanced phonon mediated superconductivity. Phys Rev B. 2016;93:144506.
[92] Bittner N, Tohyama T, Kaiser S, et al. Light induced superconductivity in a strongly correlated electron system. arXiv: 1706.09366v1; 2017.